Hindawi
Advances in Materials Science and Engineering
Volume 2020, Article ID 5189473, 7 pages
https://doi.org/10.1155/2020/5189473

Research Article

Residual Stresses Formed by Vibration-Centrifugal Hardening

Yaroslav Kyryliv,[1] **Volodymyr Kyryliv**,[2] **Nataliya Sas**,[3] **and Volodymyr Dutka**[3]

[1]*Lviv State University of Life Safety, Kleparivska St., 35, Lviv 79007, Ukraine*
[2]*Karpenko Physico-Mechanical Institute of the NAS of Ukraine, Naukova Str., 5, Lviv 79060, Ukraine*
[3]*Stepan Gzhytskyi National University of Veterinary Medicine and Biotechnologies, Pekarska Str., 50, Lviv 79010, Ukraine*

Correspondence should be addressed to Yaroslav Kyryliv; yaroslav_kyryliv@ukr.net

Received 19 November 2019; Revised 19 January 2020; Accepted 13 February 2020; Published 14 March 2020

Academic Editor: Georgios Maliaris

The residual stresses of the first kind, which are formed by vibration-centrifugal hardening, are calculated. These are shown to increase in the hardened layer with increasing processing time and the weight of the hardening tool. The residual compressive stresses in the hardened layer after vibration-centrifugal hardening for optimal parameters reach maximum values: circular stresses up to $\sigma_{\text{cir}}^{\max} = 1600$ MPa and radial stresses up to $\sigma_r = 290$ MPa. Their correlation with surface microhardness is shown.

1. Introduction

Physicomechanical properties of metals, such as fatigue, fretting fracture, wear resistance, and cavitation erosion resistance, depend on residual stresses of the first kind in the surface layers formed during operations of finishing processing. Therefore, the optimization of the surface layer properties is of great importance for improving the performance of machine parts. In this regard, new technologies for treating metal surfaces based on the formation of nanocrystalline structures (NCSs) and ultrafine-grained structures (UFGSs) in the surface layers are of great interest. In particular, one of the ways to form the NCS and UFGS is to grind grains in the surface layer of a massive material to nanometer sizes. Previous studies have shown that the NCS and UFGS can be formed, in particular, using severe plastic deformation (SPD) of the surface. In particular, when the NCS and UFGS are formed on the surface, its chemical composition can be changed [1] and it protects the matrix material from hydrogen saturation [2], corrosion [3], wear [4], and contact fatigue [5]. One of the methods for the UFGS formation is vibration-centrifugal hardening (VCH) [6–8]. It is shown [6–8] that VCH due to the significant weight of the strengthening tool forms a UFGS of high microhardness and considerable (up to 7 mm) depth.

In the developed VCH method, the processing regimes can be used to control the parameters of the hardened layer, in particular, the tool weight over a wide range (from 3.5 to 7.5 kg) with a constant diameter of the balls. Such conditions change the depth and microhardness of the surface layer due to changes in contact loads in the treatment zone [6, 7]. This ensures fragmentation of the surface layer structure and increases its imperfection, which leads to an improvement in its (surface layer) properties. When applying the vibration methods of processing, the main parameters that affect the physicomechanical properties of the surface layer are the amplitude and frequency of oscillations, the weight of the tool, the diameter of the balls, and the processing time. In particular, the VCH, as well as other SPD methods, forms residual compressive stresses. The formation of the nature and magnitude of the residual stresses in the surface layers of hardened machine parts by the VCH has not been studied.

The aim of this work is to study and calculate the magnitude of the residual stresses under optimal conditions of the VCH on 40 kh steel.

2. Materials and Methods

The 40 kh steel with the chemical composition shown in Table 1 taken from the certificate material was used. Samples—rings with an outer and an inner diameter of 75 and 60 mm, respectively, and a width of 20 mm—were made from it by turning. To relieve residual stresses after turning, the samples were annealed, heating them to a temperature of 820°C and cooling with a furnace for 8 hours. Work hardening was carried out on a special vibration-centrifugal strengthening device [6] with a special massive tool with balls of 13 mm in diameter fixed on it.

The installation (see Figure 1) provides vibrations of a certain amplitude and revolving of the tool and its movement along the machined cylindrical surface. Under the influence of vibration, the tool rotates and moves along the forming part of the treated workpiece. The frequency of rotation of the tool around the axis of the workpiece depends on the frequency and amplitude of the oscillations. At each moment of time, the tool contacts one of the balls with the surface of the workpiece. The contact of the next ball comes with a blow, and the bodies that collide are a massive tool and a part. The impact interaction of the tool with the part during their contact through the ball forms large contact stresses in the surface layer of the material of the part at the points of contact with the ball. The material of the component is hardened as a result of the SPD. The design of the tool and its weight make it possible to obtain high contact loads with constant sizes of balls and also provide a fixed direction of movement of the balls fixed in a cage in the radial direction to the workpiece, which increases the depth of work hardening [6]. Balls made of ShKh15 steel have a hardness of HRC 60-62. The samples were fixed on a mandrel. Processing parameters were as follows: amplitude of oscillations $A = 5$ mm; oscillation frequency $f = 24$ Hz; weight of the working tool $m = 3.5$, 4.5, and 7.5 kg; processing time $t = 6$, 12, 20, 28, and 36 min; and eccentricity $\varepsilon = 10$ mm.

One of the known methods for determining residual stresses after the SPD [9] is the method that consists in work hardening the sample's outer surface in the form of a ring with its subsequent cutting and measuring the displacement at the section. If the thickness of the hardened layer is the same, we can assume that a uniformly distributed radial load q is formed in its contact with the base metal of the sample. Under its influence, internal force factors arise that determine the mutual displacement of the ring sections after the cut.

After the VCH, cylindrical samples were removed from the mandrel and fixed in a special device. Two cuts were made on the samples on the outer surface, perpendicular to the lateral surfaces, at half the depth of the ring in two places at a distance of 10 mm. The distance between them was measured with a caliper and cut to the end. Both cuts were directed to the center of the ring. After cutting out a part of the ring, it was compressed by the value Δ_{km}, with which the residual stresses were determined.

To determine the microhardness and depth of the hardened layer of hardened samples, PMT-3 microhardness testers were used. Tests were carried out by indentation of a standard 136-degree Vickers diamond pyramid indenter with a square base at a load of 100 g. Microhardness was determined by the formula

$$H_\mu = \frac{1854P}{d^2}, \tag{1}$$

where P is the load and d is the diagonal of the square print.

X-ray studies of the obtained structure were carried out on an X-ray diffractometer DRON-3 in CuKα radiation ($U = 30$ kV, $I = 20$ mA) with a step of 0.05° and the exposure at point 4 s. The diffractograms were processed using the CSD software package [10]. The X-ray patterns were identified by JCPDS-ASTM card files [11]. The microstructure was investigated on an EVO 40XVP scanning electron microscope.

Table 1: Chemical composition of 40 kh steel.

Steel grade	Content of elements (%)							
	C	Si	Mn	Cr	S	P	Cu	Ni
40 kh	0.41	0.29	0.63	0.98	0.032	0.031	0.3	0.3

3. Results and Discussion

Let us consider in more detail the internal force factors arising with a radially uniformly distributed load q. In Figure 2 [9], a diagram of a ring of arbitrary shape cut along a symmetry plane, which, in a closed form, is a statically indefinite system, is presented. A radial load q acts on its contour, and the internal force factors X_1, X_2, X_3, X_4, X_5, and X_6, which may occur in its cross sections, are as yet unknown values.

From the symmetry condition [12], the transverse force $X_3 = X_5 = 0$. Bending moments X_1 and X_4 can be determined using the least work theorem [12].

$$\frac{\partial W}{\partial X_1} = 0, \qquad \frac{\partial W}{\partial X_4} = 0, \tag{2}$$

where W is the potential energy, which is determined by the dependence

$$W = \frac{1}{2}\int_0^l \frac{M(s)\mathrm{d}S}{EI(s)}, \tag{3}$$

where $M(s)$ is the bending moment in any cross section of the ring, which is considered; dS is the elementary length of the axis of the ring section; $I(s)$ is the axial moment of inertia of the cross section of the ring; and l is the length of the axis of the half-ring.

The bending moment in the cross section with the i point with a coordinate y_1 is determined by the expression

$$M(s) = X_1 - X_2 y_1 + 2qa_1 b_1, \tag{4}$$

all designations of which are given in Figure 2. The dotted line in this figure shows the position of the neutral axis. If we add the equilibrium condition with respect to point C of the lower section, we obtain

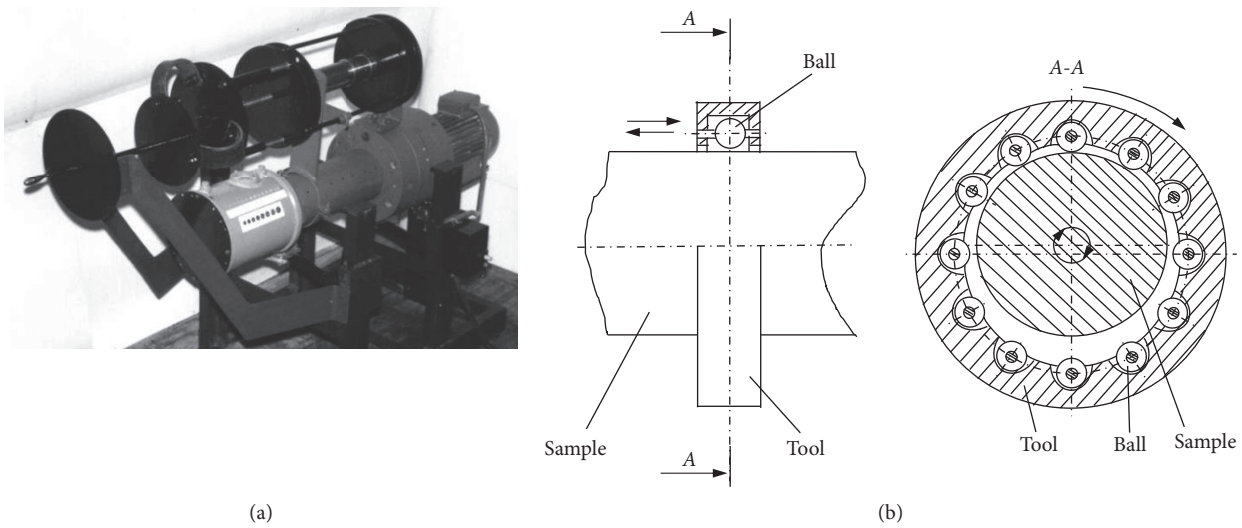

Figure 1: Installation for vibration-centrifugal hardening (a) and schematic representation of a process (b).

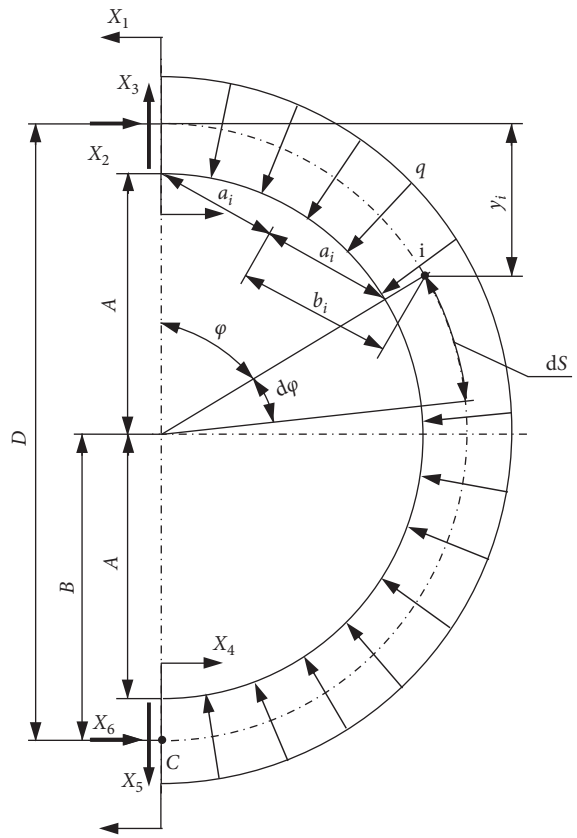

Figure 2: Calculation scheme of the ring with a radial load acting on its circuit.

$$X_4 - X_1 + X_2 D - 2qAB = 0, \tag{5}$$

or from here, we have

$$X_2 = \frac{X_1 - X_4}{D} + 2qA\frac{B}{D}. \tag{6}$$

Substituting (6) into expression (4), we get

$$M(s) = 2qAB\left(\frac{a_1 b_1}{AB} - \frac{y_1}{D}\right) + X_1\left(1 - \frac{y_1}{D}\right) + X_4\frac{y_1}{D}. \tag{7}$$

Using dependence (3) with respect to (7), we find an expression for the potential energy, and then, by determining the partial derivatives of formula (2), we obtain a system of equations for finding unknown X_1 and X_4. If we consider the system for a special case, when the ring is a circle with the radius r and the ring is thin (the height of the cross section is small compared to the radius), then

$$\begin{aligned} a_1 &= b_1 = r\sin\frac{\phi}{2}, \\ y_1 &= r(1 - \cos\phi), \\ A &= B = r, \\ D &= 2r. \end{aligned} \tag{8}$$

In this case, the solution of the equations leads to the following values: $X_1 = X_4 = 0$. Then, substituting (8) in (6), we obtain $X_2 = 2qA(B/D) = qr$. This means that if the ring is a circle of small thickness, then, as a result of the action of the hardened layer in all its cross sections, only longitudinal force will arise, which after the cut will move the ring gradually by some value Δ_{km} (see Figure3).

Thus, the value of the contact load q [9] can be determined by measuring displacements in the Δ_{km} direction after cutting the sample. To determine theoretically the named displacement, we use the Mohr integral, which allows us to find any displacements of the points of the elastic systems.

It is known that if the transverse force is neglected, the Mohr integral will take the form [13]

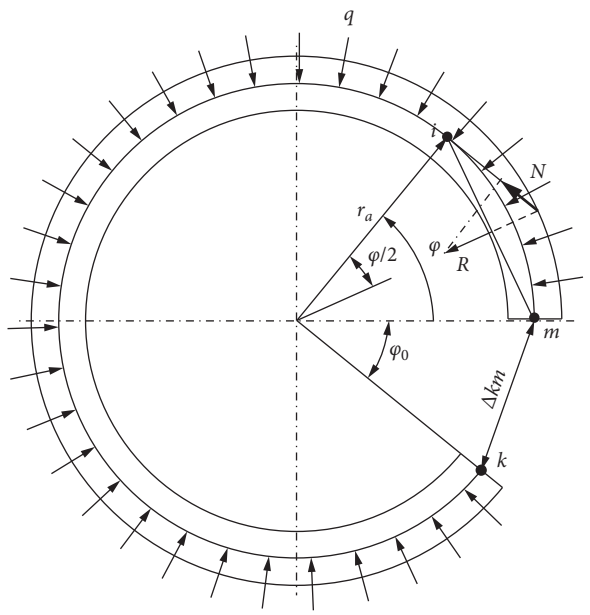

Figure 3: Diagram of the loaded state of the ring.

$$\Delta_1^1 = \sum \int M_1 \frac{M}{EI} \mathrm{d}S + \sum \int N_1 \frac{N}{EF} \mathrm{d}S. \tag{9}$$

M_1 and N_1 are analytical expressions for bending moment and longitudinal force in an arbitrary cross section, resulting from a unit force applied at a point, whose movement is determined. In this case, a unit force should be applied in the direction of the desired displacement. M and N are analytical expressions for bending moment and longitudinal force in an arbitrary cross section that arise under the action of external loads. In our case, the external load is q. In Figures 3 and 4, diagrams of unit and external loads, respectively, are shown. From Figure 4, it follows that [9]

$$\begin{aligned} M_1 &= -1h = 2r_a \sin\frac{\phi}{2} \sin\left(\frac{\phi + \phi_0}{2}\right), \\ N_1 &= \cos\left(\frac{\phi + \phi_0}{2}\right). \end{aligned} \tag{10}$$

From Figure 3, we get $M = 2qr_a^2 \sin(\phi/2)$ and $N = -2qr_a \sin^2(\phi/2)$.

Substituting these values in (9) and integrating in the range from $\varphi = 0$ to $\varphi = 2\pi - \varphi_0$, and also replacing the uniformly distributed load q by the pressure p, which it creates per unit area of the contact surface, we obtain [9]

$$\Delta_{km} = \frac{12pr_a^4}{E(r_o - r_i)^3}(\lambda + \mu) - \frac{pr_a^2}{E(r_o - r_i)}(\eta - \mu), \tag{11}$$

where $p = q/b$ is the pressure on the contact of the hardened layer and the ring, in which b is the ring width; r_a is the average radius of the ring; and r_o and r_i are the outer and inner radii of the ring, respectively.

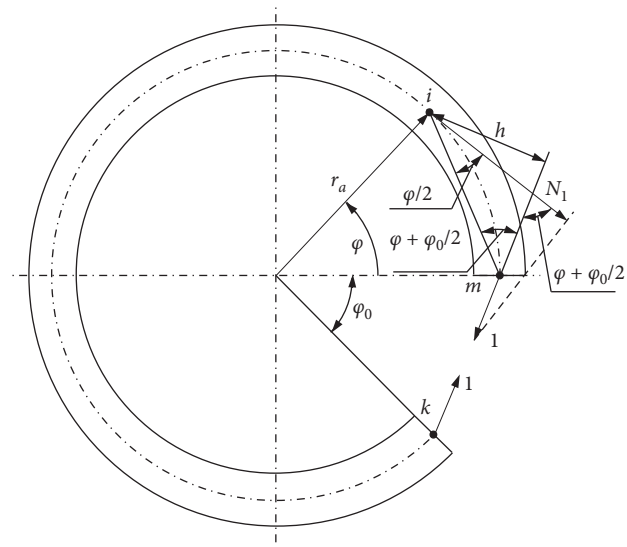

Figure 4: Unit load diagram of the ring.

$$\begin{aligned} \lambda &= \cos\frac{\phi_0}{2}\left(3\pi - 1,5\phi_0 + 2\sin\phi_0 - 0,25\sin 2\phi_0\right), \\ \mu &= \sin\frac{\phi_0}{2}\left(1 - \cos\phi_0 + 0,5\sin^2\phi_0\right), \\ \eta &= \cos\frac{\phi_0}{2}\left(-\pi + 0,5\phi_0 - \sin\phi_0 + 0,25\sin 2\phi_0\right). \end{aligned} \tag{12}$$

From (11), we get the following formula for determining the contact pressure, which is formed under the influence of the hardened layer [9]:

$$p = \frac{E\Delta_{km}}{\left(12r_a^4/t^3\right)(\lambda + \mu) - \left(r_a^2/t\right)(\eta - \mu)}, \tag{13}$$

where $t = r_o - r_i$ is the ring section height.

Using the theory of calculation of multilayer pipes [14], one can now determine the radial and circular stresses at the points of the hardened layer. Figure 5 shows the load diagram of the hardened layer, where it can be seen that it is subjected to internal pressure p, which is determined by equation (13). In this case, the radial and circular stresses at any point belonging to the hardened layer are determined by the dependence

$$\sigma_{r_{cir}} = \frac{r_2^3 p}{r_1^2 - r_2^2}\left(1 \mp \frac{r_1^2}{\rho^2}\right), \tag{14}$$

where r_1 and r_2 are the outer and inner radii of the hardened layer and ρ is the distance from the center of the ring to the point under consideration.

The greatest circular stress, which follows from the analysis of equation (14), occurs on the inner surface of the hardened layer, where $\rho = r_2$, and will be equal to

$$\sigma_{cir}^{max} = p\frac{r_1^2 + r_2^2}{r_1^2 - r_2^2}. \tag{15}$$

The radial stress at these points is $\sigma_r = -p$. Using formula (14), it is possible to determine the radial and circular

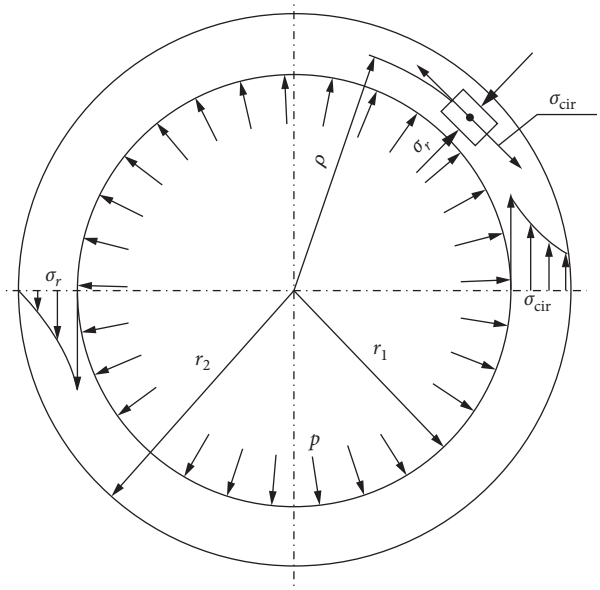

Figure 5: Scheme for the calculation of stresses in the hardened layer.

stresses, which, for the case under consideration, are simultaneously the main stresses [9].

Thus, the analytical dependences make it possible to calculate the residual stresses in the hardened layer by changing the cut (Δ_{km}) of the circular sample, allowing for the analysis of their magnitude and purposeful change in the VCH conditions.

Based on the obtained analytical dependence (14), the resulting residual stresses formed in the hardened material layer are calculated.

Calculation results are shown in the corresponding graphs (see Figure 6).

The graphs show that, for 40 kh steel, with an increase in the deformation force and the duration of work hardening, the level of residual radial and circular stresses (see Figure 6) in the material hardened layer increases. This is consistent with the theory of elastoplastic deformation of the material, according to which an increase in the deformation force with a constant contact area leads to an increase in contact stresses, which partially transform into residual stresses.

An increase in the level of residual compressive stresses with an increase in the processing time is explained by the increase in the number of repeated metal deforming impacts for each individual unit of the hardened surface area. As known, dynamic repeated deformation of the material, unlike static deformation, is accompanied up to a certain period of time not only by an increase in the diameter of the imprint formed by the impact of the working tool but also by the increase in the depth of work hardening as a result of the SPD. At the same time, the stress-strain state of 40 kh steel grows, and the value of the residual stresses associated with it increases. The residual stresses in the hardened layer after explosive treatment with a processing time of $\tau = 28$ min reach their maximum values: circular compressive stresses at $\sigma_{cir}^{max} = 1600$ MPa and radial compressive stresses at $\sigma_r = 290$ MPa. A further increase in the duration of work hardening as a result of reriveting of the metal and the accompanying stress relaxation reduces the compressive stresses, formed in the hardened layer of the material.

It has been established that the optimal processing conditions, from the point of view of ensuring maximum values of residual stresses, are as follows: $A = 5$ mm, $m = 4.5$ kg, $\tau = 28$ min, and $\varepsilon = 10$ mm. The minus sign for radial stresses indicates that these stresses are compressive stresses. The correlation between microhardness and residual compressive stresses (see Figure 7) is shown under optimal processing conditions. This is also confirmed by the microstructure obtained from the studied samples of the starting material and after the VCH (see Figure 8) under optimal conditions at a depth of 100 μm [6]. The X-ray analysis also established the relative microdeformations of the crystal lattice along the depth of the sample (see Figure 9) under the optimal conditions given above and showed their correlation with microhardness, which obviously indicated the presence of residual stresses. In addition, the VCH under favorable conditions forms residual compressive stresses of the first kind, which are balanced within the part or a section of its surface.

It was shown in [15–17] that residual compressive stresses slowed down the formation and growth of fatigue cracks. Thus, the residual compressive stresses in the region of local plastic deformations will retard the fracture processes that occur, as a rule, with the formation of residual tensile stresses. The experimental results indicate a rather uniform distribution of the residual compressive stresses depending on the variable parameters of the VCH process, which is in good agreement with the distribution of microhardness over the surface layer thickness. In the as-received samples, the surface microhardness is 2.2 GPa and reaches up to 8.9 GPa under optimal conditions of VCH. It can be assumed that such a hardened layer should have a strong bond with the metal base. This is important for the operation of machine parts subjected to high

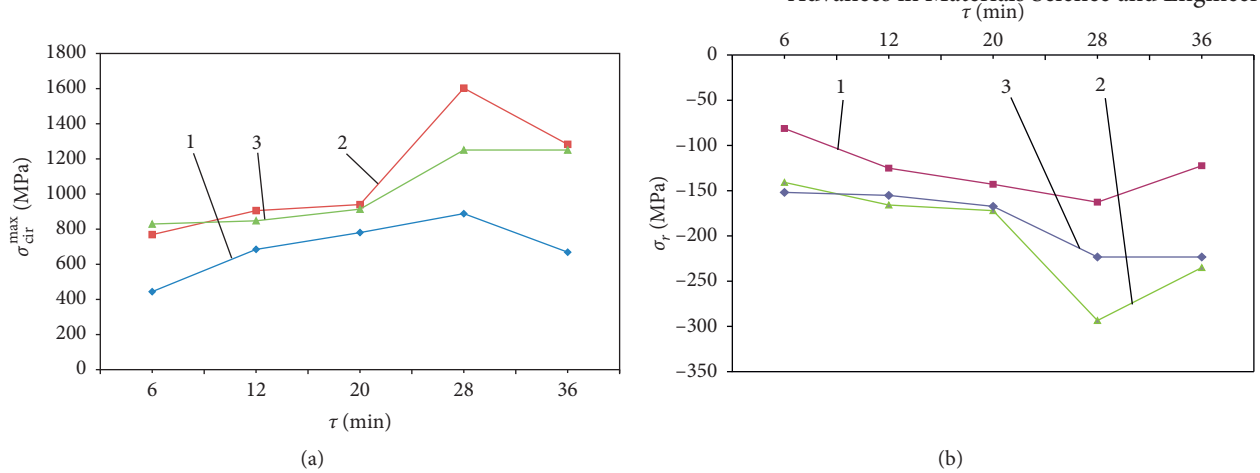

FIGURE 6: Dependence of the magnitude and sign of the residual stresses in the hardened layer after VCH on the processing time and weight of the hardened tool. 1, 3.5 kg; 2, 4.5 kg; 3, 7.5 kg. (a) Circular compressive stresses σ_{cir}^{max}. (b) Radial compressive stresses σ_r.

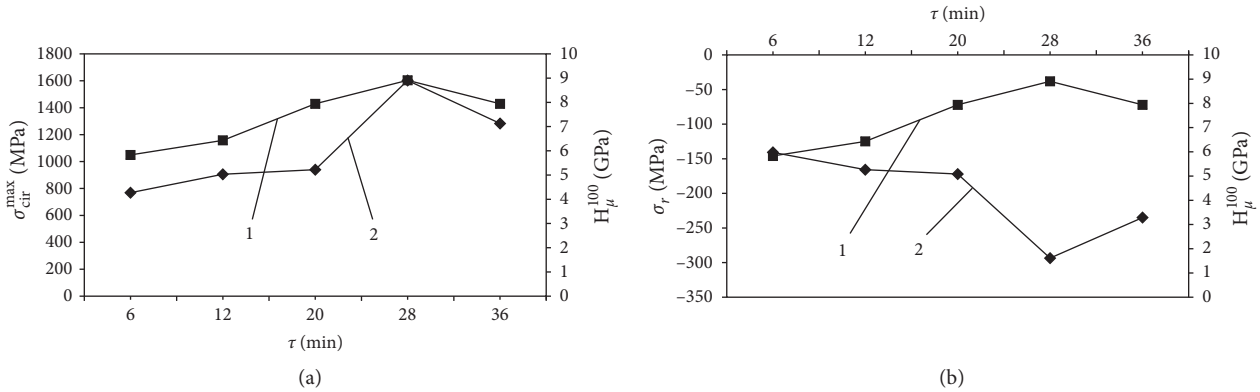

FIGURE 7: Dependence of the microhardness (1) and the magnitude and sign of the residual stresses (2) in the hardened layer after explosive treatment on the processing time with the weight of the hardened tool 4.5 kg: (a) circular compressive stresses, σ_{cir}^{max}; (b) radial compressive stresses, σ_r.

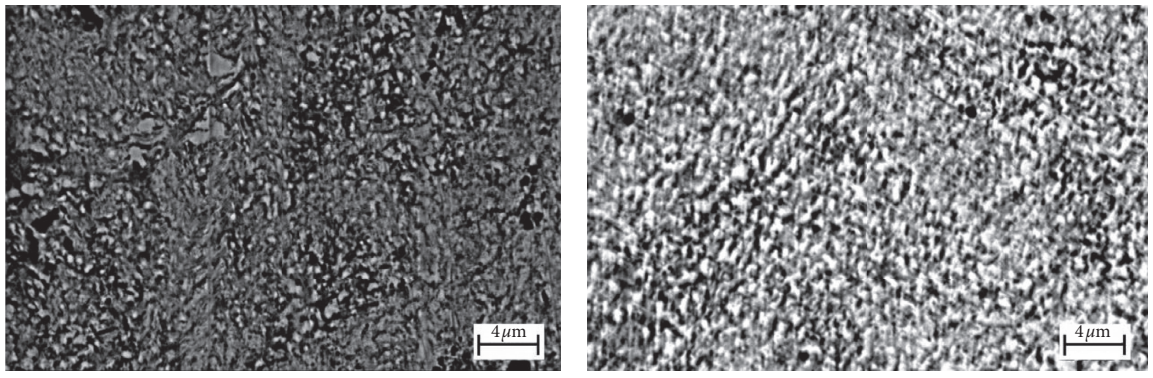

FIGURE 8: Structure of 40 kh steel with optimal parameters after VCH at (a) 100 μm depth and (b) the initial lattice structure.

dynamic loads. It can be seen from the obtained results that the residual compressive stresses depend not only on the microhardness of the surface layer but also on its depth.

So, the VCH forms in the surface layers the residual compressive stresses of the first kind, which depend on the processing conditions and, under optimal conditions, reach circular stresses of 1600 MPa and radial stresses of 290 MPa.

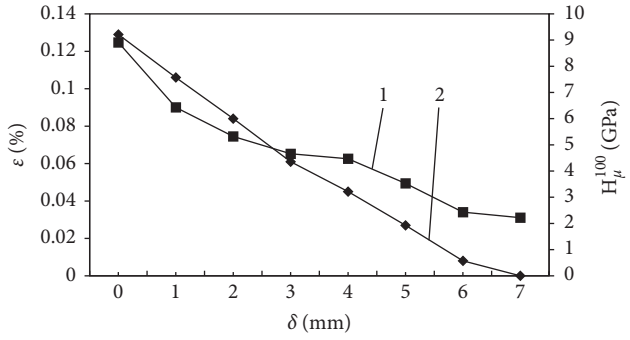

Figure 9: Distribution of microhardness (1) along the depth of the hardened sample δ and the relative microdeformation of the crystal lattice (2) after VCH with a processing time of 28 min and a weight of the hardening tool of 4.5 kg.

4. Conclusions

(1) The VCH forms in the surface layer the residual compressive stresses of the first kind, which depend on the processing conditions. Under processing conditions, $m = 4.5$ kg, $\tau = 28$ min, and the maximum residual stresses are ensured for 40 kh steel: circular compressive stresses at $\sigma_{\text{cir}}^{\max} = 1600$ MPa and radial compressive stresses at $\sigma_r = 290$ MPa.

(2) It is shown that the residual compressive stresses (both circular and radial) correlate with surface microhardness.

Data Availability

The data used to support the findings of this study are available from the corresponding author upon request.

Conflicts of Interest

The authors declare that there are no conflicts of interest regarding the publication of this paper.

Authors' Contributions

YK developed a study chart, performed general analysis of the results, and prepared the paper. He calculated residual stresses, both radial and circular. VK selected a method for calculating residual stresses and adapted it to the calculation of the obtained results. He performed cutting of the samples and then measured their movement. NS measured and calculated the microhardness and the relative microdeformation of the crystal lattice of the hardened layer using physical research methods. In addition, she built the calculation schemes. VD measured the movement of the cut samples under the influence of stresses. He also constructed the graphical dependences of the obtained results. All authors read and approved the final text of the manuscript.

References

[1] V. I. Kyryliv, "Surface saturation of steels with carbon during mechanical-pulse treatment," *Materials Science*, vol. 35, no. 6, pp. 853–858, 1999.

[2] H. Nykyforchyn, E. Lunarska, V. Kyryliv, and O. Maksymiv, "Influence of hydrogen on the mechanical properties of steels with the surface nanostructure," *Springer Proceedings in Physics*, vol. 167, pp. 457–465, 2015.

[3] H. Nykyforchyn, V. Kyryliv, O. Maksymiv, Z. Slobodyan, and O. Tsyrulnyk, "Formation of surface corrosion-resistant nanocrystalline structures on steel," *Nanoscale Research Letters*, vol. 11, no. 1, p. 6, 2016.

[4] H. Nykyforchyn, V. Kyryliv, and O. Maksymiv, "Effect of nanostructurisation for structural steels on their wear hydrogen embittlement resistance," *Solid State Phenomena*, vol. 225, pp. 65–70, 2015.

[5] V. Kyryliv, B. Chaikovs'kyi, O. Maksymiv, and B. Mykytchak, "Fatigue and corrosion fatigue of the roll steels with surface nanostructure," *Journal of Nano Research*, vol. 51, pp. 92–97, 2018.

[6] V. Kyryliv, Y. Kyryliv, and N. Sas, "Formation of surface ultrafine grain structure and their physical and mechanical characteristics using vibration-centrifugal hardening," *Advances in Materials Science and Engineering*, vol. 2018, Article ID 3152170, 7 pages, 2018.

[7] Y. Kyryliv, V. Kyryliv, and N. Sas, "Influence of surface ultrafine grain structure on cavitation erosion damage resistance," *Springer Proceedings in Physics*, vol. 221, pp. 97–107, 2019.

[8] I. S. Aftanaziv, A. I. Bassarab, and Y. B. Kyryliv, "Mechanical and corrosion characteristics of 40 kh steel after vibration-centrifugal hardening treatment," *Materials Science*, vol. 38, no. 3, pp. 436–441, 2002.

[9] B. P. Skvortsov and Y. A. Sidorenko, "Calculation of residual stresses in an isothermal sprayed layer," *Collection of Scientific Papers of the Belarusian Agricultural Academy*, pp. 28–35, 1984.

[10] W. Krous and G. Nolze, "Powder cell–a program for the representation and manipulation of crystal structures and calculation of the resulting X-ray powder patterns," *Journal of Applied Crystallography*, vol. 29, no. 3, pp. 301–303, 1996.

[11] L. G. Akselrud, P. Y. Zavalii, Y. N. Grin, V. K. Pecharski, B. Baumgartner, and E. Wölfel, "Use of the CSD program package for structure determination from powder data," *Materials Science Forum*, vol. 133–136, pp. 335–342, 1993.

[12] A. Blake, *Practical Stress Analysis in Engineering Design (Revised and Expanded Second Edition)*, Marcel Dekker, New York, NY, USA, 1990.

[13] R. Hulse and J. Cain, *Structural Mechanics: Worked Examples*, Macmillan International Higher Education, New York, NY, USA, 2009.

[14] M. Farshad, "Determination of the long-term hydrostatic strength of multilayer pipes," *Polymer Testing*, vol. 24, no. 8, pp. 1041–1048, 2005.

[15] E. Sonde, T. Chaise, D. Nelias, and V. Robin, "Numerical simulation of electromagnetic surface treatment," *Journal of Applied Physics*, vol. 123, no. 4, Article ID 045901, 2018.

[16] S. Zabeen, M. Preuss, and P. J. Withers, "Residual stresses caused by head-on and 45° foreign object damage for a laser shock peened Ti-6Al-4V alloy aerofoil," *Materials Science and Engineering: A*, vol. 560, pp. 518–527, 2013.

[17] E. Brinksmeier, J. T. Cammett, W. König, P. Leskovar, J. Peters, and H. K. Tönshoff, "Residual stresses-measurement and causes in machining processes," *CIRP Annals*, vol. 31, no. 2, pp. 491–510, 1982.